J Math Chem (2015) 53:220–235
DOI 10.1007/s10910-014-0423-0

ORIGINAL PAPER

The fast-time instability map of Liñán's diffusion-flame regime

Vladimir Vladimirovich Gubernov · Jong Soo Kim

Received: 7 March 2014 / Accepted: 26 September 2014 / Published online: 8 October 2014

Abstract A detailed spectral map for the fast-time instability in Liñán's diffusion-flame regime is presented in order to clarify the origin of two bifurcations of co-dimension 2, causing the transitions from cellular to uniform-oscillatory instability and from uniform-oscillatory to traveling instability. The role of the real and continuous essential spectrum is found to be pivotal in understanding both transitions. Particular attention is paid to the spectral characteristics in the stable parametric regions, where the interaction with the essential spectrum leads to these transitions. When the Lewis number is increased above unity from below, the discrete real spectrum disappears by submerging below the essential spectrum, and the discrete complex spectrum emerges instead, eventually leading to uniform-oscillatory instability. The transition from uniform-oscillatory to traveling instability, associated with the Bogdanov–Takens bifurcation, involves a phenomenon called gap spectrum. For Lewis numbers slightly greater than unity and Damköhler numbers sufficiently large, the discrete complex spectrum intersects the plane corresponding to the essential spectrum, resulting in a gap in the discrete spectrum for small wave numbers. The discrete complex gap spectrum exhibits a local maximum as the parameter values are modified to approach the Hopf bifurcation boundary. The gap in the discrete complex spectrum disappears and traveling instability emerges when crossing the Hopf bifurcation boundary.

V. V. Gubernov (✉)
P.N. Lebedev Physical Institute of Russian Academy of Science, 53 Leninskii prospect, Moscow 119991, Russia
e-mail: gubernov@lpi.ru

V. V. Gubernov
ICE Lab., Far Eastern Federal University, 8, Sukhanova Str., Vladivostok 690950, Russia

J. S. Kim
Energy and Environment Research Division, Korea Institute of Science and Technology, PO Box 131, Cheongryang, Seoul 130-650, Korea

Keywords Activation energy asymptotics · Liñán's diffusion-flame regime · Fast-time instability · Oscillatory instability · Bogdanov–Takens bifurcation

1 Introduction

The fast time instability is a particular class of intrinsic flame instabilities with the length and time scales of the inner reactive–diffusive layer rather than the conventional flame scales based on the outer convective–diffusive layer. In the context of activation-energy asymptotics (AEA) [1], where the Zel'dovich number β, a ratio of the activation energy to the thermal energy, serves as the large expansion parameter, the inner reactive–diffusive layer is thinner than the outer convective–diffusive layer by an order of magnitude in the Zel'dovich number, and the corresponding time scale is two-orders-of-magnitude shorter. Since perturbations involve much shorter wavelengths, the corresponding growth or decay is much faster and so arrives the name, fast-time instability.

The fast-time instability, excluding the transport processes pertinent to the convective–diffusive layer, becomes a purely reactive–diffusive problem. Consequently the fast-time instability is the most succinct flame-instability formulation and its results should be universally applicable to reactive–diffusive instabilities occurring in laminar flames. Since the modification of the instability spectrum, associated with the convective transport, is needed only for small wave numbers of $O(\beta^{-1})$, the results for fast-time instability can be regarded as the baseline characteristics for flame instability.

Although it has been long since the first analysis of fast-time instability by Peters [2], the papers, concerning the spectral nature of the fast-time instability, are rather limited to those by Kim et al. [3–5] on diffusional–thermal instability of diffusion flames. In particular, the recent papers by Gubernov and Kim [4,5], carried out for $L < 1$ and $L > 1$, respectively, mapped the parametric regions exhibiting distinct instability spectra by systematically examining the dispersion relations in the parametric space of L and Δ' where L is the common Lewis number for fuel and oxidizer and Δ' denotes the logarithmic derivative of the reduced Damköhler number Δ with respect to the inner reactant leakage, as a measure for the degree of chemical non-equilibrium.

The first paper by Kim and Gubernov [4] was devoted to the cellular instability occurring for $L < 1$. The unstable spectra were found for $\Delta' > 0$. The case of $\Delta' = 0$ is obviously the minimum Δ condition, indeed corresponding to the static extinction for flames with $L = 1$. However, for flames with $L < 1$, extinction is shifted to a positive value of Δ', due to the excess-enthalpy phenomenon arising from the condition of the chemical energy influx being greater than the thermal energy outflux. Consequently, there is a window of opportunity for cellular instability to occur even after crossing the condition of $\Delta' = 0$.

The analysis in [5], carried out for $L > 1$, reveals a more complex instability map. First of all, the nature of instability is oscillatory, as manifested by the complex eigenvalues, but the detailed nature differs depending on the Lewis number L. For Lewis numbers greater than unity but yet smaller than a critical value L_c, the instability is found to be uniform and oscillatory, and its onset occurs through the saddle-node

bifurcation immediately after crossing the instability boundary. However, for Lewis numbers greater than the critical value L_c, the corresponding instability is found to occur in a multi-stage manner. Traveling instability occurs first upon crossing the Hopf bifurcation boundary, and further increase of Δ' brings in a series transition leading to uniform-oscillatory instability via traveling instability that is observable only in a narrow parametric region of Δ'. In particular, the critical condition at $L = L_c$ and $\Delta' = \Delta'_c$, that is responsible for the transition from the uniform-oscillatory instability to traveling instability, is identified as the Bogdanov–Takens bifurcation.

As a whole, the fast-time instability exhibits three different routes to enter the unstable regions, namely cellular, uniform-oscillatory and traveling instabilities. The switching between these instability types is due to the bifurcations of co-dimension 2 at $L = 1,\ \Delta' = 0$ and at $L = L_c,\ \Delta' = \Delta'_c$. The first bifurcation is commonly observed in many flame instability situations, and is relatively well understood. However, the detailed procedures for the latter bifurcation are yet to be fully understood although the qualitative differences in the dispersion relations in the regions around the Bogdanov–Takens bifurcation condition are partially known. Particularly, we are more concerned with the qualitative differences in stable dispersion relations. The Previous work by Gubernov and Kim [5] exhibited that crossing the line of $L = L_c$ from below makes two distinct changes in stable dispersion relations, namely $Re(S) \neq 0$ at $K = 0$ and non-monotonic variation of $Re(S)$ with K, whereas stable dispersion relations below $L = L_c$ are firmly anchored at $Re(S) = 0$ and $K = 0$ and $Re(S)$ decrease monotonically. Such qualitative transformations of the dispersion relation in the stable region would be linked to the origin of Bogdanov–Takens bifurcation. It is therefore our purpose of this research to investigate the spectral characteristics of the eigenvalues in the stable regions to understand the detailed procedure for the Bogdanov–Takens bifurcation to emerge.

2 Conservation equations

The detailed derivation steps for the conservation equations are not presented here and the final equations for the mean field as well as unsteady field will be written here directly. The readers would be referred to the previous paper by Kim, Williams and Ronney [3] for the detailed derivation.

2.1 The structure equation for the mean field

The mean-field inner structure is described by the famous Liñán's canonical equation for the diffusion-flame regime written below [1]

$$\frac{d^2\Theta}{d\xi^2} = \Delta(\Theta - \xi)(\Theta + \xi)\exp\{-(\Theta + \gamma\xi)\}, \qquad \Theta_\xi \to \pm 1 \quad \text{as} \quad \xi \to \pm\infty \tag{1}$$

where Θ is the inner variable for the temperature profile and ξ is the inner coordinate. The fuel and oxidizer concentrations are given through the coupling relationships as

$$\Theta_F = \Theta - \xi, \qquad \Theta_O = \Theta + \xi. \tag{2}$$

The factor γ measures the degree of asymmetry in the thermal diffusion across the reaction zone and all the numerical results presented in this paper are obtained for $\gamma = 0$, that can be one of the most representative cases for the diffusion-flame regime. In addition, Δ is the reduced Damköhler number and will be just called Damköhler number for notational brevity unless specifically mentioned otherwise. The mean-field problem in Eq. (1) is posed as that of finding the Θ profile as a function of Δ.

The overall characteristics of the mean-field solution could be better represented by the C-shaped curve of $\Delta(\alpha)$ where the reactant leakage α is defined to be $\alpha = \Theta_F(\xi \to \infty) \equiv (\Theta - \xi)(\xi \to \infty)$. The C-shaped curve possesses a minimum value of Δ, denoted by Δ_m, below which solutions to Eq. (1) do not exist. The condition of minimum Δ is a saddle-node bifurcation point (or otherwise called turning point), in the vicinity of which interesting dynamic behaviors are anticipated to arise.

Since the instability characteristics is directly linked to the state of reaction, we employ the logarithmic derivative of Δ with respect to α,

$$\Delta' \equiv \frac{d \ln \Delta}{d\alpha} \tag{3}$$

as the reaction-state variable, mainly because of its particular properties. In the Burke–Schumann limit corresponding to $\Delta \to \infty$, $\Delta' \to -\infty$. With increasing α, Δ' keeps monotonically increasing whilst $\Delta' = 0$ at the turning point, thereby the sign of Δ' serving as a convenient indicator of whether the reaction state passes the turning point or not. The value of Δ' can be directly computed with a better accuracy from the eigenvalue problem for Δ', that can be derived by simply taking partial derivative of Eq. (1) with respect to α. The behavior of the eigenvalue Δ' can be found in [3,6].

2.2 The conservation equations for the linear instability analysis

In order to examine the stability of the inner reactive–diffusive structure, its time dependent response on perturbations, imposed on the mean-field solution, is considered. With the simplification of the Lewis numbers identical for the both fuel and oxidizer, the differential equations describing the time-dependent behavior of an infinitesimally small normal-mode perturbation are written as

$$\frac{d^2\psi}{d\xi^2} - (S + K^2)\,\psi = \frac{d^2\chi}{d\xi^2} - (LS + K^2)\,\chi = \Delta e^{-(\Theta+\gamma\xi)}[2\Theta\chi - (\Theta^2 - \xi^2)\psi\,] \tag{4}$$

where ψ and χ are the eigenfunctions for the inner-zone temperature and fuel (or oxidizer) variables, respectively, S is the growth rate and K is the wave number. The differential equations in Eq. (4) are subject to the boundary conditions $\psi \to 0$ and $\chi \to 0$ as $\xi \to \pm\infty$, from matching with the outer region, where the perturbations are found to be vanishing at the leading order. This matching condition arises from the vanishing perturbations outside of the inner layer since the perturbations are too fast and too short for them to survive in the outer layer.

Even if the vanishing perturbation is a correct matching condition, it is often impractical to impose the strong boundary condition, because it requires too big a calculation domain for the eigensolution to converge to the imposed boundary condition. Therefore, we rather employ a weaker boundary condition given as

$$\frac{d\psi}{d\xi} \to \mp\sqrt{S+K^2}\,\psi, \quad \frac{d\chi}{d\xi} \to \mp\sqrt{LS+K^2}\,\chi, \quad \text{as } \xi \to \pm\infty \tag{5}$$

representing the exponential decay toward the boundary region.

The stability problem is posed as that of finding the growth rate S as a function of the wave number K for the specified values of L and Δ'. The key tool that is used for the numerical investigation of stability of diffusion flames is the Evans function method [7]. Previously the Evans function approach was employed to study the onset of pulsating instabilities in premixed flames with Lewis number $L > 1$ for both the adiabatic [8] and nonadiabatic flames [9,10]. In our earlier studies [4,5], we also extended the applicability of the method to investigate the instabilities of a different nature, namely cellular and oscillatory instabilities in diffusion flames, which are dominant for $L < 1$ and $L > 1$, respectively.

2.3 Essential spectrum

For $L = 1$, Eq. (4) gives $\chi = \psi$, and a classical eigenvalue problem, similar to that of Schroedinger type, is obtained,

$$\frac{d^2\psi}{d\xi^2} + (E - V)\,\psi = 0, \quad \psi(\pm\infty) = 0. \tag{6}$$

with "energy" $E = -(S + K^2)$ and "potential" $V(\xi) = \Delta(2\Theta - \Theta^2 + \xi^2)e^{-(\Theta+\gamma\xi)}$ [11]. Since $V \to 0$ as $\xi \to \pm\infty$, it is known that there is a continuum of eigenvalues E for $E \geq 0$ and while a discrete number of eigenvalues may exist for $E < 0$ [11,12]. Seen from the nature of Eq. (6) similar to that of the wave equation, Eq. (6) will exhibit an oscillatory behavior in the region where $(E - V) > 0$. Particularly if $(E - V) > 0$ toward the infinitely extended boundaries, a continuous spectrum of eigenfunctions, which gradually decay to the ξ-axis while oscillating across the axis, are permitted. Consequently, $S < -K^2$ becomes the essential spectrum for Eq. (6).

Although $V(\xi) > 0$ if $|\xi|$ is sufficiently large, the solution to Eq. (1) has a range of ξ over which $V(\xi) < 0$, for the branch of solutions $\Theta(\xi)$ that has the greater amount of leakage. Consequently, negative but yet discrete eigenvalues E can be found for $\Delta' > 0$ and these negative values of E correspond to instability ($S > 0$) at sufficiently small values of K. Interest centers on the least stable solutions, that is, on the largest negative eigenvalues E, and the eigenfunctions ψ for these lowest energies have no zeros for finite values of ξ. For these solutions, $S = -E - K^2$ is maximum for $K = 0$ and negative for $K > \sqrt{-E}$. Buckmaster, Nachman and Taliafero [13] addressed this problem for $K = 0$ and concluded that the lower branch of the C-shaped curve, in

which $\Delta' < 0$, is stable, with instability setting in at the turning point, $\Delta' = 0$. The same conclusion clearly applies even if transverse diffusion ($K \neq 0$) is permitted. The negative slope of the straight line of S as a function of K^2 demonstrates the stabilizing influence of transverse diffusion in the reaction zone. In contrast to the results for $L < 1$ with convective–diffusive scaling, stability now always is encountered at sufficiently large K.

For $L \neq 1$, the coupling relationship $\psi = \chi$ is no longer valid, and the eigenvalue problem in Eq. (4) takes a somewhat different form,

$$\{D_{\xi\xi} + (\mathbf{E} - \mathbf{V})\}(\psi, \chi) = 0, \quad (\psi, \chi)(\pm\infty) = 0, \tag{7}$$

where the energy matrix $\mathbf{E}$ and potential matrix $\mathbf{V}$ are given as

$$\mathbf{E} = \begin{bmatrix} -(S + K^2) & 0 \\ 0 & -(LS + K^2) \end{bmatrix} \quad \mathbf{V} = \Delta e^{-(\Theta + \gamma\xi)} \begin{bmatrix} -(\Theta^2 - \xi^2) & 2\Theta \\ -(\Theta^2 - \xi^2) & 2\Theta \end{bmatrix}. \tag{8}$$

In the above equation for the potential matrix $\mathbf{V}$, we can immediately note that $\mathbf{V}$ is no longer self-adjoint, thereby permitting complex eigenvalues, which are in fact found for $L > 1$. Although the eigenvalue problem in Eqs. (7) and (8) does not fall into the classical Schroedinger equation, its eigenvalues and eigenfunctions have to follow the similar mathematical behaviors subject to the eigen-pair to Eq. (6). Since the potential $\mathbf{V}$ exponentially decays to "0" as $\xi \to \pm\infty$, $E_\psi = -(S + K^2) > 0$ and $E_\chi = -(LS + K^2) > 0$ corresponds to the essential eigenvalue spectrum for ψ and χ, respectively. Once a continuous spectrum appears in either space of E_ψ or E_χ, the continuous spectrum should be permitted. The continuous spectrum $S < -K^2/\max(L, 1)$ is the region where the essential eigenvalue spectrum for Eq. (4) lies.

Although the above arguments do not possess mathematical rigor and rather appeal to physical intuition it can be shown that they are indeed correct. We rewrite the Eqs. (7) and (8) in a form of a system of differential equations of the first order as

$$\mathbf{u}_\xi = \mathbf{A}(\xi, \lambda)\mathbf{u}, \quad \mathbf{A}(\xi, \lambda) = \begin{bmatrix} 0 & \mathbf{I} \\ -(\mathbf{E}(\lambda) - \mathbf{V}(\xi)) & 0 \end{bmatrix} \tag{9}$$

where $\mathbf{u} = [(\psi, \chi), (\psi, \chi)_\xi]^\mathbf{T}$ and $\mathbf{I}$ is a 2×2 identity matrix. It is known that the properties of the eigenvalue problem (7) and (8) are closely related to the spectral characteristics of the limit matrix $\mathbf{A}(\lambda) = \lim_{\xi \pm\infty} \mathbf{A}(\xi, \lambda)$. According to [14], parameter S belongs to the essential spectrum if $\mathbf{A}(\lambda)$ is not hyperbolic. It can be easily demonstrated that the latter condition is satisfied if S is real and either $S + K^2 < 0$ or $LS + K^2 < 0$. Therefore we again conclude that the essential spectrum is contained in the region of all real S satisfying the condition $S < -K^2/\max(L, 1)$. For further analysis, it is convenient to imagine the essential spectrum in three dimensional space of (ReS, ImS, K) as a half plane $ImS = 0$ located below the line $ReS = -K^2/\max(L, 1)$.

3 Spectral characteristics in the stable regions

In this section, our attention will be focused mainly on the spectral characteristics in the stable regions, particularly in order to illuminate the origin of the Bogdanov–Takens bifurcation. The numerical calculations are carried out along the four parametric trajectories, marked in Fig. 1, in which the subplots exhibit typical behaviors of the primary discrete spectra for distinct $L - \Delta'$ parametric regions. In the subplots, the solid lines represent the real discrete spectrum while the dashed lines represent the complex discrete spectrum.

Prior to examine the spectral characteristics, it is quite useful to summarize the previous results as a baseline information to the present study. In Fig. 1, the stable region for $L < 1$ is found to be located in the region of $\Delta' < 0$ with the instability boundary plotted by the thick solid line. The transition occurs through the emergence of positive real eigenvalues in a range of small wave numbers, thereby giving rise to a cellular instability. For $L > 1$, the boundary between the stable and unstable regions is marked by a thick solid line and a thick dashed line, each corresponding to the saddle-node bifurcation associated with uniform-oscillatory instability and the Hopf bifurcation associated with traveling instability, respectively. These three boundary segments separating the unstable region from the stable region correspond to bifurcation of co-dimension 1. On the other hand, the two transition points between three boundary segments, occurring at $L = 1$, $\Delta' = 0$ and $L = L_c$, $\Delta' = \Delta'_c$, correspond to bifurcation of co-dimension 2. In particular, the second transition, marked by the asterisk sign in Fig. 1, is known as the Bogdanov–Takens bifurcation, associated with the transition from the saddle node bifurcation to the Hopf bifurcation. For more detailed description of Fig. 1, we refer the readers to the previous works carried out by the authors [4,5]. The parametric trajectories, along which the numerical calculations are carried out, are specifically chosen to investigate variation of the spectral characteristics around the bifurcations of co-dimension 2.

First we examine the spectral characteristics along the line '1' for which the Lewis number L is fixed at 0.8 while Δ' is gradually increased from -0.6 to 0.0 at which the cellular instability is allowed to emerge. The spectral variation along the line '1' is depicted in Fig. 2, where the shaded region corresponds to the essential spectrum $S < -K^2/\max(L, 1) = -K^2$. The primary spectrum for $L < 1$ is always real and is found to lie above the essential spectrum. The essential spectrum and primary spectrum converge to each other only at the origin $S = K = 0$. As known from the previous analysis [3,4], as long as $\Delta' \leq 0$, the growth rate S increases gradually with increasing Δ' although remaining negative for all wave numbers. In Fig. 2, the curve 5, corresponding to $\Delta' = 0$, possesses the property of $S = 0$ and $dS/dK^2 = 0$ at $K = 0$, the condition stating the onset condition of instability. Once Δ' becomes positive, the growth rate S is permitted to take a positive value for a finite range of small wave numbers, which is not shown in Fig. 2. Qualitative variation of the spectral characteristics for $L = 0.8$ beyond $\Delta' > 0$ can be seen from Fig. 1. Initially crossing through the line of $\Delta' = 0$, the growth rate $S(K = 0)$ remains to be 0 while possessing a positive value for dS/dK at $K = 0$. However, further increase of Δ' beyond a critical value at $\Delta' = 1 - L$ causes even planar waves to become unstable as seen from Fig. 1 that $S(K = 0)$ is no longer attached at the origin $S = K = 0$.

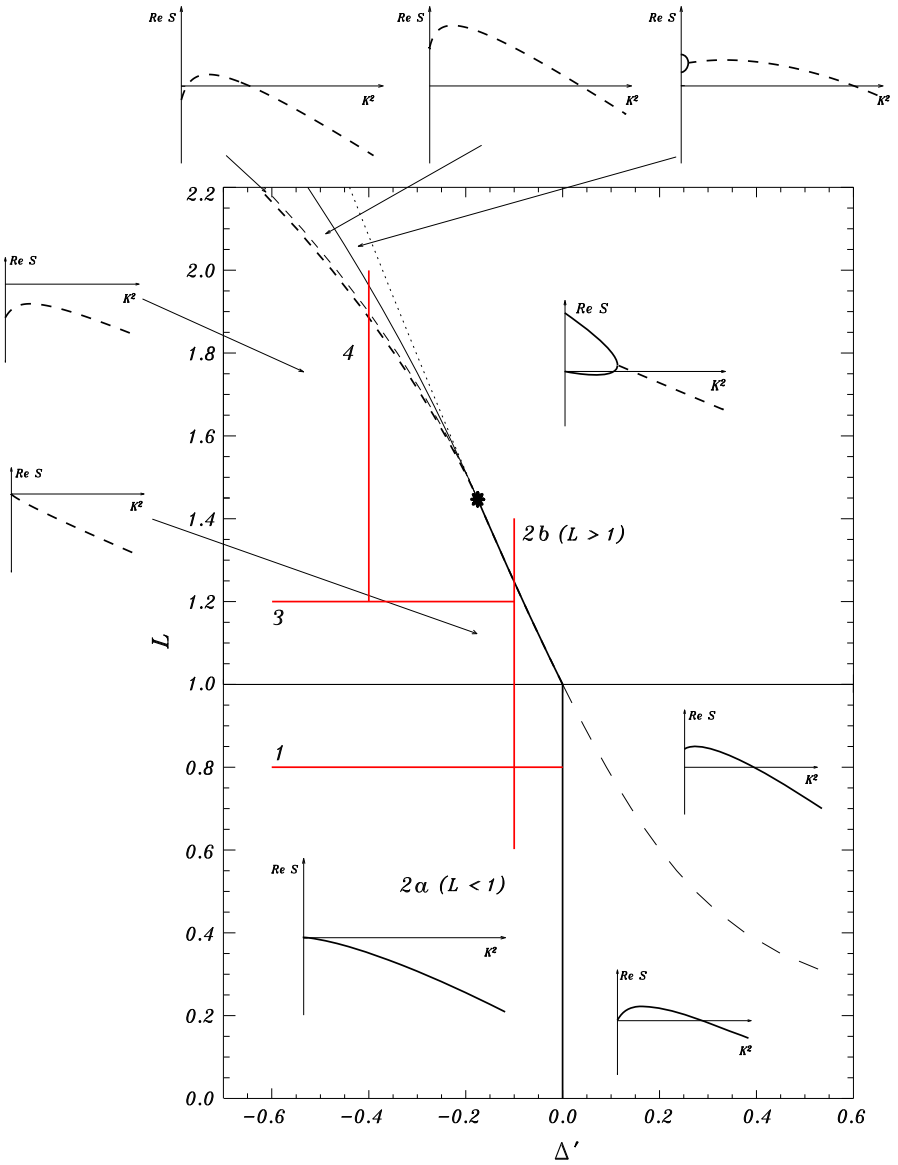

Fig. 1 Stability diagram based on the previous studies [4,5] and the trajectories along which the spectral characteristics will be examined

Now we examine variation of the spectral characteristics with L along the trajectory '2' in Fig. 1. Since the trajectory '2' spans the Lewis number L from 0.6 to 1.4 while Δ' is fixed at -0.1, the trajectory is divided into two parts, namely, the trajectories '2a' and '2b', each corresponding to $L \leq 1$ and $L \geq 1$, respectively. The characteristics of spectral variation along the trajectory '2a' is shown in Fig. 3, in which the essential spectrum again corresponds to $S < -K^2$ as Fig. 2 and is shaded. Since Δ' is negative,

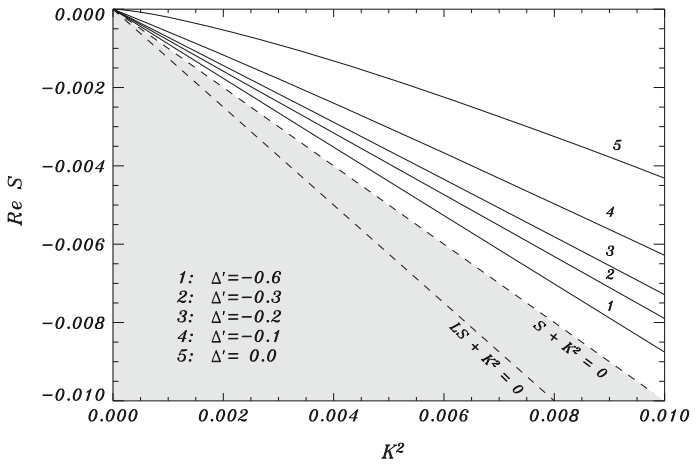

Fig. 2 The real dispersion relations $S(K^2)$ for $L = 0.8$ and various values of Δ'

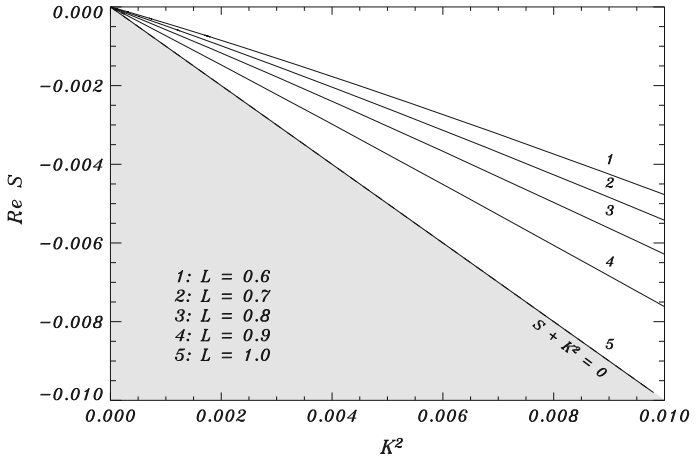

Fig. 3 The real dispersion relations $S(K^2)$ for $\Delta' = -0.1$ and various values of $L \leq 1$

i.e. before reaching the instability onset condition and $L \leq 1$, the growth rate is real negative for all wave number. However, with the Lewis number L increasing toward unity, the growth rate S is decreasing for all wave numbers while still anchored at $S = K = 0$. At $L = 1$, the primary spectrum becomes $S + K^2 = 0$, which finally collapse with the essential spectrum, indicating that a completely different spectral nature will emerge as the Lewis number L goes above $L = 1$.

As the Lewis number L becomes greater than unity, the spectral characteristics are examined for the trajectory '2b', along which a great change occurs for the essential spectrum. Since the essential spectrum is $S < -K^2/\max(L, 1)$, the region for the essential spectrum expands with L increasing above unity. In order to describe the spectral characteristics in association with the essential spectrum, the vertical axis is now modified from S to LS. Therefore, it is possible to fix the upper boundary of the

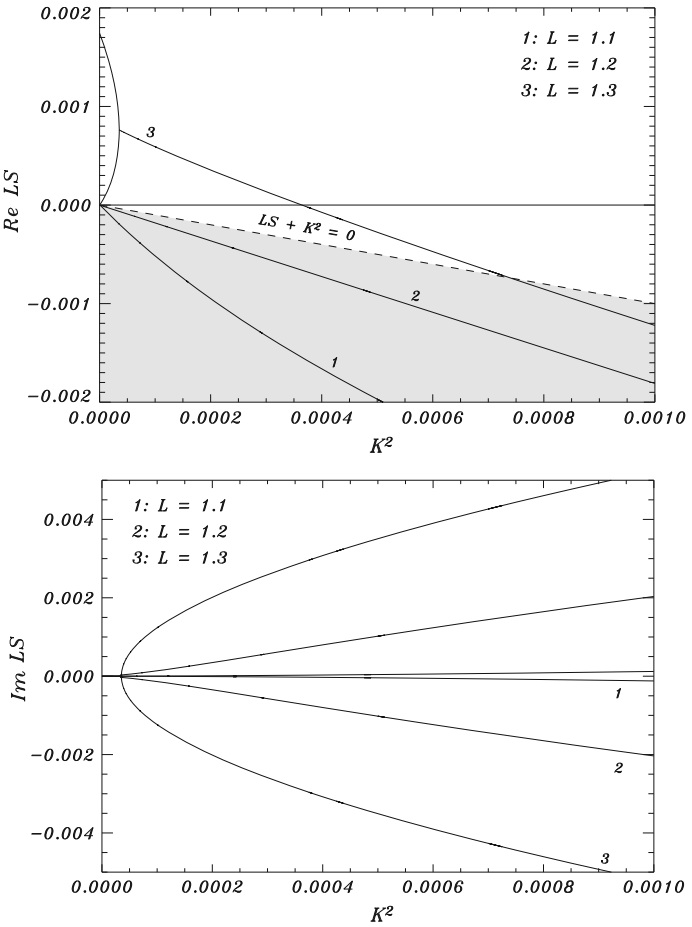

Fig. 4 Real and imaginary parts of the dispersion relations $LS(K^2)$ for $\Delta' = -0.1$ and various values of L

essential spectrum while maintaining the qualitative nature of dispersion relations. As the Lewis number L moves just above $L = 1$, the primary spectrum disappears from the region above the essential spectrum and discrete spectra with a different nature appears. The curve 1 in Fig. 4, corresponding to $L = 1.1$, exhibits the discrete spectrum with the largest $Re(S)$. It has to be noted that the largest eigenvalue is found in the upper boundary of the essential spectrum and that the discrete spectrum is complex as seen from the imaginary part depicted in the lower plot of Fig. 4 and is allowed to be separated from the essential spectrum even if $Re(S)$ falls below $LS < -K^2$. As the Lewis number is further increased to $L = 1.2$, but yet before crossing the instability onset boundary, the real part of the discrete spectrum tends to move upward in $Re(LS)$ shown in the curve 2 of the upper plot of Fig. 4 as well as $Re(S)$ not shown in the figure. The imaginary part is much greater for $L = 1.2$ than that of $L = 1.1$, indicating that the oscillatory nature is strengthened.

Just below $L = 1.3$, the trajectory '2b' now crosses the instability onset boundary, marked by the thick solid line. The curve 3 corresponds to the primary spectrum for $L = 1.3$, which is composed of the real and complex branches. For sufficiently small wave numbers, there exists a real branch, which is no longer single-valued. At $K = 0$, the primary real eigenvalue is positive, meaning that instability has emerged, while the secondary real eigenvalue is anchored at the origin. As the wave number increases, the primary and secondary real eigenvalues approach each other and eventually form a half loop. A double real eigenvalue exists at the rightmost turning point of the half loop and a pair of complex conjugate eigenvalues bifurcate from the turning point as seen from the curve 3 of Fig. 4. The complex conjugate pair varies in a monotonic manner in that the real part $Re(LS)$ decreases monotonically whereas the imaginary part $Im(LS)$ increases monotonically. The real part of the primary complex eigenvalue may fall below the upper boundary of the essential spectrum, but it never crosses the essential spectrum because the primary branch lies in the complex domain. The curve 4 corresponds to the case of $L = 1.4$, and its qualitative nature is identical to that of curve 3 except that the growth rate $Re(S)$ is greater for $L = 1.4$. It is worthwhile to note that the imaginary parts look different depending on how the complex eigensolution bifurcates. When the complex eigensolution comes out from the real turning point, as seen from the case of $L = 1.3$, the imaginary branch departs the axis of $Im(LS) = 0$ in a vertical manner, so that the two conjugate solution form a round edge, exhibiting a typical characteristics of the saddle node bifurcation. However, if the complex eigensolution pair come from the origin and $Re(LS)$ stays below the essential spectrum, the edge is sharply pointed, lacking the nature of saddle node bifurcation.

We now examine the spectral characteristics along the trajectory '3', where the Lewis number L is fixed at 1.2 while Δ' decreases from -0.1 to a value small enough to exhibit a distinct spectral characteristics. In Fig. 5, four different cases are presented for $\Delta' = -0.1, -0.15, -0.2$ and -0.225. For $\Delta' = -0.1$ and -0.15, the complex branches start right out from the origin and $Re(LS)$ remains below the upper limit of the essential spectrum. As discussed in the previous paragraph, the curves for $Im(LS)(K^2)$, shown in the lower plot, are pointed at the point departing from the axis of $Im(LS) = 0$. The departure angle for $Im(LS)(K^2)$ is seen to shrink with decreasing Δ'. Further decreasing Δ', the discrete spectrum for $\Delta' = -0.2$ begins to exhibit a distinct characteristics in that the discrete complex spectrum exists only for sufficiently large wave numbers, say $K^2 > 0.00503$. Below the critical wave number, the discrete spectrum crosses the plane of the essential spectrum, consisting of $Im(LS) = 0$ and $\max\{1, L\}S + K^2 < 0$, and merges into the continuous essential spectrum. Consequently, there exists a wave number gap, in which the discrete spectrum ceases to exist. The gap can be clearly observed from the curve 3 in Fig. 5. The transition to this gap behavior can be related to the edge bifurcation [15]. If Δ' further decreases to -0.225, the qualitative nature essentially remains the same with the case of $\Delta' = -0.2$, but the gap widens as seen from the curve 4 of Fig. 5. The numerical calculations were carried out up to $\Delta' = -0.6$ along the trajectory '3' in Fig. 1, but the results are shown only up to $\Delta' = -0.225$ because the gap region is too big to show in Fig. 5.

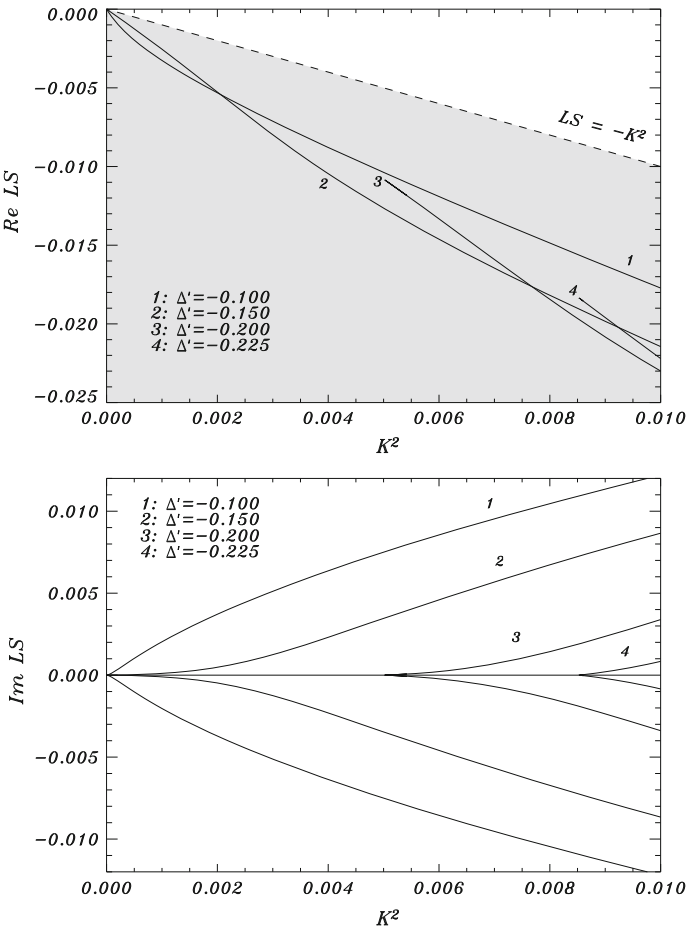

Fig. 5 Real and imaginary parts of the dispersion relation $LS(K)$ for $L = 1.2$ and various values of Δ'

Finally, we examine the spectral characteristics along the parametric trajectory '4', where Δ' is fixed at $\Delta' = -0.4$ and the Lewis number increases from 1.2 to 2.0. Since the range of S and K^2 to properly show the spectral characteristics is widely spaced, we will show only a few numerical results that can be clearly plotted in Fig. 6. In order to examine the transition sequence from the gap spectrum to oscillatory behavior, including traveling and uniform oscillatory instabilities, the Lewis number is gradually increased. The curves 1 and 2, corresponding to $L = 1.3$ and $L = 1.4$, are seen to possess the gaps, in which the discrete spectra do not exists. However, the spectra for $L = 1.3$ and $L = 1.4$ reveal an important distinction that $Re(LS)$ for $L = 1.4$ is no longer monotonic, exhibiting a maximum of $Re(LS)$ near $K^2 = 0.0075$, marked by a circle. The emergence of this maximum $Re(LS)$ is particularly important because the fundamental structure for traveling instability lies in this nonmonotonic behavior of $Re(LS)$, which is in turn associated with the origin of the Bogdanov–Takens bifurcation.

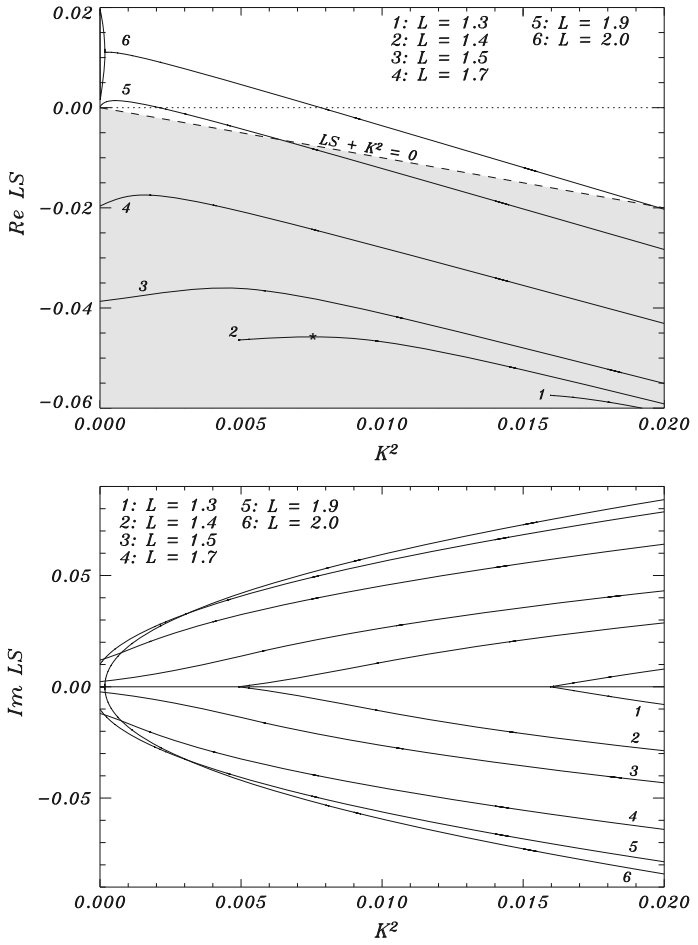

Fig. 6 Real and imaginary parts of the dispersion relations $LS(K^2)$ for $\Delta' = -0.4$ and various values of L

For $L = 1.5$ and $L = 1.7$, each shown by the curves 3 and 4, the gaps are no longer found and $Im(LS) \neq 0$ at $K = 0$ as seen from the lower plot, indicating that the discrete spectra do not cross the plane of the essential spectrum. Moreover, there remain the maximum of $Re(LS)$ along the curves 3 and 4. However, the loci of maximum $Re(LS)$ get closer to the axis of $K = 0$. For $L = 1.9$ shown by the curve 5, the spectrum still remains complex, but moves above the upper limit of essential spectrum. Moreover, the real part of the growth rate emerges above $Re(LS) = 0$ with the maximum $Re(LS)$ occurring at a finite wave number, exhibiting a typical traveling instability. Therefore, the edge bifurcation is reversed while moving the Lewis number L from 1.7 to 1.9. Further increasing the Lewis number to $L = 2.0$, the spectrum with the saddle node bifurcation, already discussed for the curve 3 in Fig. 4, appears again. It thus is shown that moving the instability control parameters L or Δ' deep into the

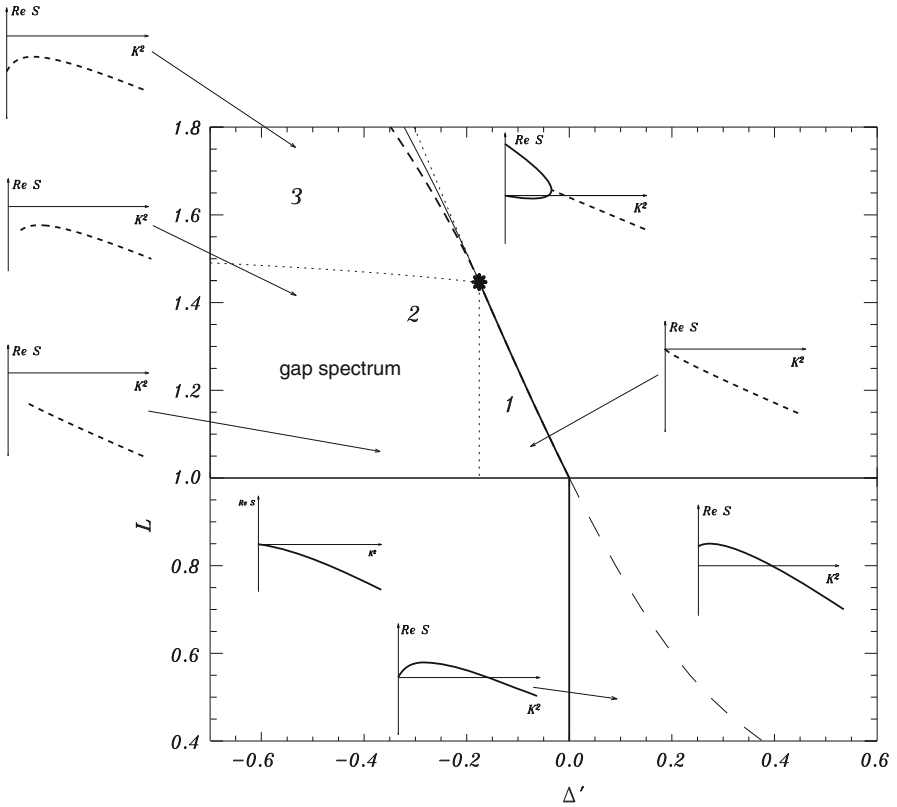

Fig. 7 The diagram mapping the regions with different spectral characteristics

unstable region by increasing either of these parameters causes the instability mode to return to the uniform oscillatory instability.

The overall diagram mapping the regions corresponding to different spectral characteristics is shown in Fig. 7. The main difference of Fig. 7 from Fig. 1 is that Fig. 7 shows extra regions with the gap spectrum. In addition, the loci for the edge bifurcation, through which the gap spectrum appears or disappears, are marked by the dotted lines in Fig. 7. In this analysis, our attention is focused on the stable region in the vicinity of the Bogdanov–Takens bifurcation, through which the transition from the saddle node bifurcation, associated with uniform oscillatory instability, to the Hopf bifurcation, associated with traveling instability, occurs. The diagram in Fig. 7 shows that there are three stable regions with different spectral characteristics. The first one corresponds to that in Fig. 4, exhibiting complex dispersion relation with a monotonically decaying real part. Upon crossing the instability boundary, the dispersion relation will be transformed into the one corresponding to uniform oscillatory instability. The second region, that is located left hand side to the first region by the edge-bifurcation boundary, is found to possess the gap spectrum. The gap spectrum can be characterized by the intersection of discrete complex spectrum with the essential spectrum, so that the discrete complex spectrum ceases to exist for a gap with small wave numbers.

More importantly, as approaching to the second edge-bifurcation boundary with the third region, the gap spectrum begins to show its local maximum of $Re(S)$, as a preparation to transform into traveling instability. Upon entering the third region by crossing the second edge-bifurcation boundary, the gap in discrete complex dispersion relation closes. The local maximum of $Re(S)$ persists, but still remains to be negative, meaning stable until crossing the Hopf bifurcation boundary, marked by the thick dashed line. When the Hopf bifurcation boundary is crossed, traveling instability emerges as shown by the curve 5 in Fig. 6. Further increasing the instability parameters, i.e L or Δ', the instability mode returns to the uniform-oscillatory mode.

4 Concluding remarks

In the previous papers by the authors, the fast-time instability occurring in the Liñán's diffusion-flame regime was systematically investigated and the regions, exhibiting different instability characteristics, ranging from cellular instability and uniform oscillatory instability to traveling instability, are mapped in the instability control parameter space of L and Δ'. The instability map reveals that there exist two bifurcation conditions with codimension 2, each marking the transition from cellular instability to uniform oscillatory instability and the transition from uniform oscillatory instability to traveling instability. In this study, our interest is focused on the investigation for the origin of these bifurcations of codimension 2 by rather examining the underlining variations of spectral characteristics in the stable regions along the trajectories delineated in Fig. 1.

In this analysis, we found that the role of essential spectrum is vital to understand the origins of the both transitions mentioned above. The essential spectrum is a real and continuous spectrum of eigensolutions, perhaps described by $\max\{1, L\}S + K^2 < 0$. Since the essential spectrum is stable, it has not attracted much attention. However, this analysis showed that interaction of the discrete spectrum with essential spectrum is responsible for transformation of the spectral characteristics.

For Lewis number less than unity, instability can occur in a cellular manner by increasing the parameter Δ'. When the Lewis number L is moved above unity from below, the discrete real spectrum disappears by submerging below the essential spectrum, and a discrete complex spectrum emerges instead. By further increasing the Lewis number L or Δ' causes the saddle node bifurcation, leading to uniform oscillatory instability. Therefore, the transition from cellular instability to uniform oscillatory instability is completed, while the transition condition is marked by a bifurcation of codimension 2 at $L = 1$ and $\Delta' = 0$.

The transition from uniform oscillatory instability to traveling instability, perhaps formally known as the Bogdanov–Takens bifurcation, involves a phenomenon called gap spectrum. For Lewis number slightly greater than unity, decreasing the parameter Δ' from the left hand side of the saddle node bifurcation boundary cause the discrete complex spectrum intersects the plane corresponding to the essential spectrum, so that the discrete complex spectrum disappears in a gap of small wave numbers. Such a transition to gap spectrum is perhaps known as the edge bifurcation. The discrete complex gap spectrum goes through a second transformation by moving slightly

toward the Hopf bifurcation boundary to have a local maximum of $Re(S)$ (though remaining negative) as preparation to traveling instability. Further moving toward the Hopf bifurcation boundary, the gap in the discrete complex spectrum disappears upon crossing the second edge-bifurcation boundary. Then, further increase of L or Δ' can cause Hopf bifurcation leading to traveling instability.

This study has been devoted the investigation of stability spectral characteristics which are found to be essential to understand the origin of different instability modes. It would quite interesting to see if the same type of bifurcations occur in different reactive–diffusive systems, including premixed-flame system and multi-step reaction system.

Acknowledgments J.S.K. would like to thank the Hydrogen Energy R&D Center (HERC), a member of the twenty-first century Frontier R&D Program organized by the Korean Ministry of Science and Technology, for their kind financial support to this research. V.V.G. would like to acknowledge the financial support from the Russian Foundation for Basic Research Grant 13-03-00282. The work was supported by the Ministry of education and science of Russian Federation (project 14.Y26.31.0003) and the FEFU Development Program.

References

1. A. Liñán, The asymptotic structure of counterflow diffusion flame for large activation energies. Acta Astron. **1**, 1007 (1974)
2. N. Peters, On the stability of Liñán's "premixed flame regime. Combust. Flame **33**, 315 (1978)
3. J.S. Kim, F.A. Williams, P.D. Ronney, Diffusional–thermal instability of diffusion flames. J. Fluid Mech. **327**, 273 (1996)
4. J.S. Kim, V.V. Gubernov, On the fast-time cellular instabilities of Liñán's diffusion flame regime. Combust. Sci. Technol. **177**, 991 (2005)
5. V.V. Gubernov, J.S. Kim, On the fast-time oscillatory instabilities of Linan's diffusion flame regime. Combust. Theory Model. **10**, 749 (2006)
6. J.S. Kim, Linear analysis of diffusional–thermal instability in diffusion flames with Lewis numbers close to unity. Combust. Theory Model. **1**, 13 (1997)
7. J.W. Evans, Nerve axon equations: III. Stability of the nerve impulses. Indiana Univ. Math. J. **22**, 577 (1972)
8. V.V. Gubernov, G.N. Mercer, H.S. Sidhu, R.O. Weber, Evans function stability of combustion waves. SIAM J. Appl. Math. **63**, 1259 (2003)
9. V.V. Gubernov, G.N. Mercer, H.S. Sidhu, R.O. Weber, Evans function stability of nonadiabatic combustion waves. Proc. R. Soc. Lond. A **460**, 1259 (2004)
10. V.V. Gubernov, G.N. Mercer, H.S. Sidhu. The effect of ambient temperature on the propagation of nonadiabatic combustion waves. J. Chem. Math. **37**, 149–162 (2005)
11. P.M. Morse, H. Feshbach, *Methods of Theoretical Physics* (McGraw-Hill, New York, 1953), pp. 766–769
12. E.C. Titchmarsh, *Eigenfunction Expansions Associated with Second-Order Differential equations* (Clarendon Press, Oxford, 1946), pp. 107–128
13. J.D. Buckmaster, A. Nachman, S. Taliaferro, The fast time instability of diffusion flames. Physica **9D**, 408 (1983)
14. B. Sandstede, Stability of travelling waves, in *Handbook of Dynamical Systems II*, ed. by B. Fiedler (North-Holland, Amsterdam, 2002), pp. 983–1055
15. G. Derks, G.A. Gottwald, A robust numerical method to study oscillatory instability of gap solitary waves. SIAM J. Appl. Dyn. Syst. **4**, 140 (2005)